ACS OMEGA

Open Access

http://pubs.acs.org/journal/acsodf

Article

First-Principles Study on the Electronic and Mechanical Properties of the Cr(001)/Al(001) Structure

Soon-Dong Park and Sung Youb Kim*

Cite This: *ACS Omega* 2023, 8, 42840−42848

Read Online

ACCESS | Metrics & More | Article Recommendations | Supporting Information

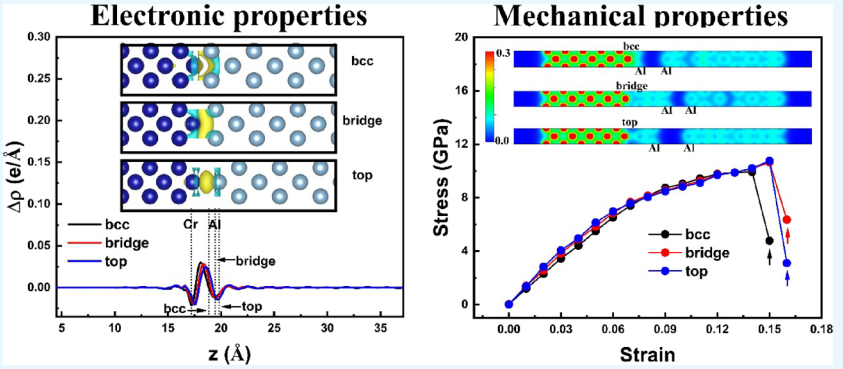

ABSTRACT: We utilized spin-polarized density functional theory to analyze the properties of the Cr(001)/Al(001) structure. The interface was classified into three forms—bcc, bridge, and top—based on the bonding coordinates between Cr and Al atoms. The total density of states (DOS) of the structures is mainly influenced by the Cr (d) orbitals. The local DOS of the Cr atoms at the interface exhibits slight variations based on their coordination with neighboring Al atoms. The mechanical properties of a specific layer were analyzed by using the rigid grain shift (RGS) method, and the properties of all layers were analyzed by using the homogeneous lattice extension method. Our results confirmed that the bonding strength, as determined by the RGS method, follows a decreasing order from the strongest to the weakest: bcc, bridge, and top. We applied uniform deformation to the entire system in the thickness direction and allowed it to relax: we observed that deformation occurs mainly in the Al region and ultimately leads to failure regardless of the type of interface. Consequently, similar strain−stress curves were observed in all Cr(001)/Al(001) structures. The failure in the Al region is attributed to the lower stiffness of the Al−Al layers compared to the top interface despite the lower work of separation for the top interface.

1. INTRODUCTION

Cr has traditionally been utilized as a coating material for decorative and protective purposes.[1] As an example of the former, in the electroplating method, a thin layer of Cr (less than approximately 2.5 μm thick) is commonly deposited onto the surface of Ni to create a lustrous appearance, which is often used for automotive parts and tools. Increasing the thickness of the Cr coating can improve the functional properties of the underlying material, such as its hardness and corrosion resistance.[2−4] However, the utilization of hexavalent Cr in electroplating has been recognized as a major environmental and human health concern.[5] To mitigate this concern, various alternatives have been proposed, including the utilization of physical vapor deposition,[6] the replacement of hexavalent Cr with trivalent Cr,[7,8] and the reduction[9] of hexavalent Cr to trivalent Cr through the use of chemical substances and photocatalyst. Recently, there have been reports highlighting the potential of Cr to serve as an electrode in miniature electronic devices, including light-emitting diodes (LEDs)[10] and solar cells.[11] A Cr−Al electrode in an LED device exhibited increased external quantum efficiency when the thickness of Cr was approximately 1 nm owing to its high ultraviolet reflectivity. Additionally, Kaltenbrunner et al. used double-layer electrodes made of Cr/CrO in flexible perovskite solar cells below ∼3 μm in size to enhance their stability.[11] The examples demonstrate the increased utilization of Cr-related interfaces at the nanoscale. This highlights the importance of understanding the nanoscale characteristics of Cr and Cr-related interfaces. Numerous first-principles studies have been conducted on pure Cr[12−15] and interfaced Cr.[16−18] However, there is a discrepancy between the experimentally derived and theoretically calculated magnetic arrangements of Cr in its

Received: August 8, 2023
Revised: October 17, 2023
Accepted: October 20, 2023
Published: November 3, 2023

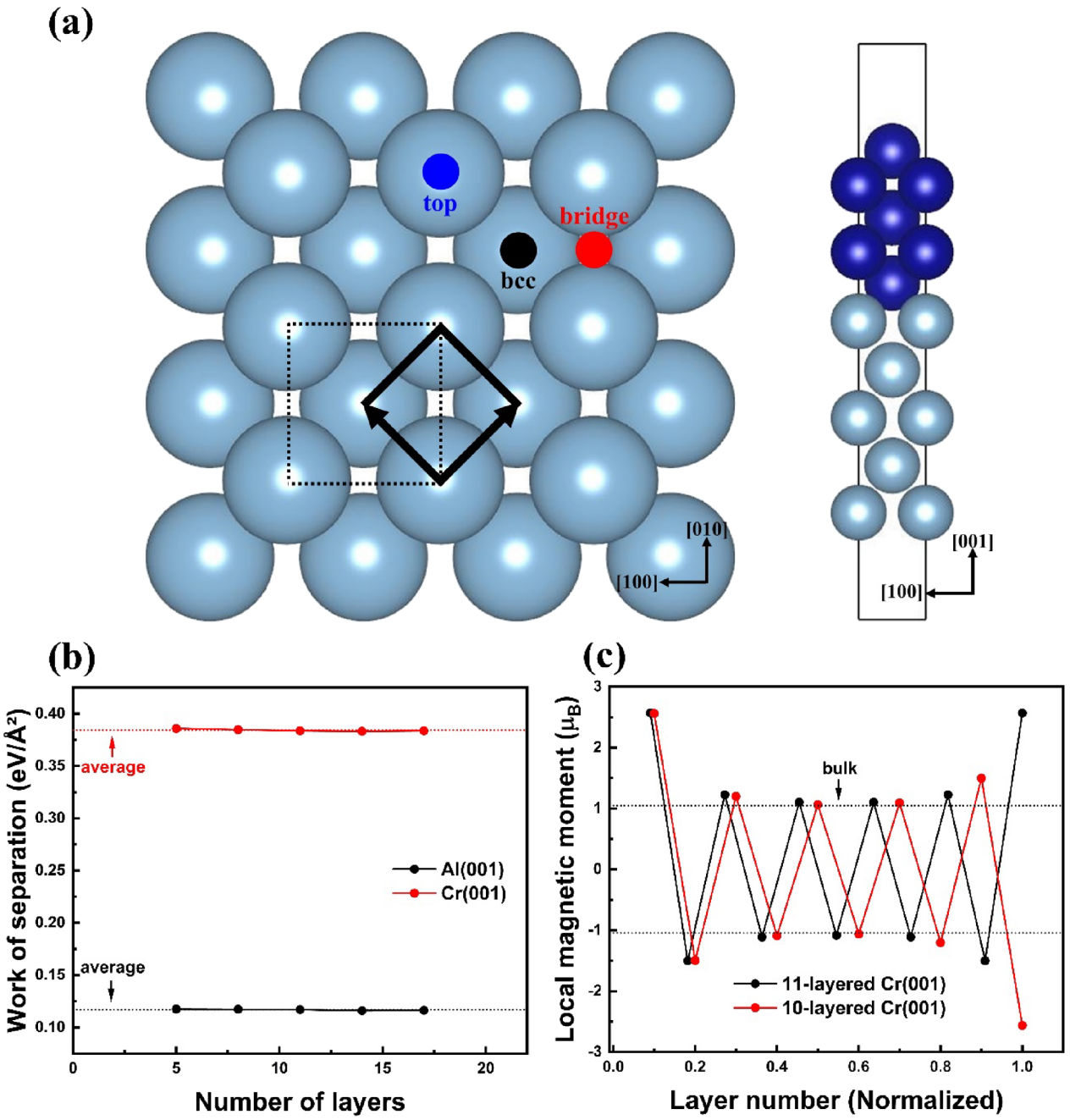

Figure 1. (a) Top view of the atomic configuration of the Al(001) slab with possible adsorption sites (bcc, bridge, and top sites) for the Cr atom. The primitive cell, which is indicated by a solid arrow in the left figure, is employed to construct the Cr(001)/Al(001) interface depicted in the right figure (a side view of the bcc-type interface). The conventional unit cell for the Al(001) slab is represented by a dashed line. (b) WS for Cr(001) and Al(001) with different numbers of layers. (c) Local magnetic moment in each layer of an 11-layered Cr(001) slab. The Cr and Al atoms are represented by dark blue and light blue spheres, respectively.

equilibrium state. An incommensurate antiferromagnetic (AF) spin density wave (SDW) with the wave vector $2\pi/a$ (0.952, 0, 0) in body-centered cubic (bcc) Cr was experimentally confirmed.[19] This phenomenon can be explained by the nesting properties of the Fermi surface and is commonly observed as the magnetic ground state below the Néel temperature. Unfortunately, theoretical methodologies face challenges in precisely predicting the properties of the SDW in Cr, unless a lattice of sufficient size is employed.[20,21] Therefore, in this study, the calculations were performed under the assumption that Cr has simple AF characteristics, with the wave vector $2\pi/a$ (1, 0, 0). Despite previous theoretical research on various interfaces,[16−18,22−24] there is a lack of reports on the interface between Cr and Al atoms. The interfaces of complex structures, such as Cr_2O_3, have been recently examined via simulations. However, owing to the requirement of a large number of atoms for modeling, these studies have been limited to analyzing characteristics such as electronic structure, bond strength, and atomic diffusion.[25−27] Therefore, the objective of the present study was to establish an ideal junction between bcc Cr and face-centered cubic (fcc) Al and subsequently analyze the relevant characteristics. In addition, owing to crystal symmetry, the junction between bcc and fcc can form structures of bcc(001)/fcc(001) and

https://doi.org/10.1021/acsomega.3c05827
ACS Omega 2023, 8, 42840−42848

bcc(110)/fcc(111). In this study, we focused on the clean Cr(001)/Al(001) structure without considering the lattice mismatch and impurities to better elucidate the characteristics of the Cr−Al junction structure and to reduce computational costs.

2. COMPUTATIONAL METHOD

We performed density functional theory (DFT) calculations to examine the electronic and mechanical characteristics of the interface between Cr(001) and Al(001). We employed spin-polarized DFT implemented using the Vienna Ab initio Simulation Package (VASP).[28,29] We used the projector-augmented wave (PAW) method to deal with the interaction between ions and electrons.[30] The correlation-exchange functional used in this study was the generalized gradient approximation (GGA) parametrized via the Perdew−Burke−Ernzerhof (PBE) method.[31] We considered the simple AF property of the Cr structure, with a local magnetic moment of approximately ±1.05 μ_B. The wave functions of electrons were set to 500 eV in energy using a plane-wave basis set. The atomic positions of pure bulk bcc Cr and fcc Al were fully optimized using a force tolerance of 0.01 eV/Å for the ions. The relaxation of the slab and interface structure was conducted in a direction perpendicular to the surface, while the lattice was fixed in the remaining directions. A Monkhorst−Pack grid with a 31 × 31 × 31 *k*-point mesh was used for relaxation of the bulk structure.[32] For optimization of the slab and interface configuration, a 31 × 31 × 1 *k*-point mesh was utilized. To create the pure slab and interface configuration, a 1 × 1 primitive cell was employed, as shown in the left frame of Figure 1a, with periodic boundary conditions imposed along the in-plane direction. The plate and interface structures were created by applying vacuum conditions in a direction perpendicular to the surface up to a distance of ∼20 Å, as shown in the right frame of Figure 1a.

3. RESULTS AND DISCUSSION

Prior to the construction of the Cr(001)/Al(001) joint structure, we verified our calculation parameters by computing the lattice constants and elastic coefficients of the individual solid structures: bcc Cr and fcc Al. In this study, two distinct categories of bulk Cr were identified according to their magnetic characteristics: bulk Cr exhibits either an AF property with a finite local magnetic moment of ± 1.05 μ_B or a nonmagnetic property without a local magnetic moment. The AF bulk Cr exhibits a lower energy value (approximately 0.01 eV/Å) than nonmagnetic bulk Cr. Hence, the AF characteristic of the Cr atom was assumed for Cr-related structures. The findings presented in Table 1 indicate close agreement between our results and those previously derived via theoretical[13,33−35] and experimental[36,37] approaches. The experimental data indicate that the DFT calculations for bcc Cr overestimated C_{11} and underestimated C_{12} and C_{44}.

Table 1. Calculated Lattice Constant (a), Elastic Constants (C_{11}, C_{12}, and C_{14}), and WS (W_{100}, Average Value for Considered Slabs) for bcc Cr and fcc Al

material	a (Å)	C_{11} (GPa)	C_{12} (GPa)	C_{44} (GPa)	W_{100} (eV/Å^2)
bcc Cr	2.85	443.73	56.63	88.82	0.38
	2.87[33]	449.67[13]	73.67[13]	86.00[13]	0.38[33]
	2.88[36]	391.00[36]	89.60[36]	103.20[36]	0.36[39]
fcc Al	4.04	113.66	59.61	33.95	0.12
	4.06[34]	117.50[35]	63.50[35]	35.50[35]	0.11[34]
	4.02[37]	114.30[37]	61.90[37]	31.60[37]	0.14[40]

In this study, the rotated lattice vector (indicated by the solid arrow) from the conventional unit cell (indicated by the dotted line) for the Al(001) slab was utilized to align the Cr(001) and Al(001) slabs, as shown in the left frame of Figure 1a. The Cr(001) and Al(001) slabs were optimized along the direction of their surfaces and constrained along the in-plane direction by utilizing their corresponding bulk lattice constants, which were approximately 2.85 and 2.86 Å, respectively. Figure 1b shows the relationship between the work of separation (WS) and the number of layers for Cr(001) and Al(001) slabs. The WS is equal to twice the surface energy needed to generate two identical surfaces.[38] A consistent trend of the WS values was observed in the two slabs, regardless of their thickness. The WS values for the Cr(001) and Al(001) slabs are found to be approximately 0.38 and 0.12 eV/Å^2, respectively. Thus, the Cr interlayer is stronger than the Al interlayer. These values are consistent with those reported in previous studies.[33,34,39,40] The magnetic behavior of the Cr(001) nanoplate is illustrated in Figure 1c, revealing a distinctive zigzag pattern of local magnetic moments, which was observed in a previous study.[15] The outermost layer exhibits a relatively high local magnetic moment due to the unpaired valence electrons of the surface atoms, while the deeper layer exhibits a value similar to that of the bulk. The total magnetic moment of the Cr(001) slab is nearly zero when it contains an even number of layers. In contrast, the Cr(001) slab with an odd number of layers exhibits a total magnetic moment of approximately 3.92 μ_B.

To form the coherent interface between the Cr(001) and Al(001) slabs, an evaluation was performed to compare the total energy for three in-plane lattices: one obtained from bulk Cr, one obtained from bulk Al, and their average, as shown in Table S1. The utilization of the lattice constant from the bulk Cr resulted in the formation of a more stable Cr(001)/Al(001) structure; thus, a compression of ∼0.14% along the in-plane direction was applied to the Al(001) slab for further study. As shown in the left frame of Figure 1a, optimization was performed for three Cr−Al interfaces: bcc, bridge, and top. On the Al(001) surface is in a bcc state, and the position denoted as bcc refers to the bonding of a Cr atom with four Al atoms, while the bridge involves bonding with two Al atoms, and the top involves bonding with only one Al atom. These interface structures were modeled by using the identical layers from each Cr(001) and Al(001) slab. The interatomic distances between Cr and Al atoms were similar among all of the cases; they were calculated as 2.60, 2.65, and 2.61 Å for the bcc, bridge, and top interfaces, respectively. The results shown in Figure 2a reveal a significant variation in the WS values among the three interface configurations. The equation for calculating the WS between Cr(001) and Al(001) is

$$W_{\mathrm{Cr}(001)/\mathrm{Al}(001)} = (E_{\mathrm{Cr}(001)} + E_{\mathrm{Al}(001)} - E_{\mathrm{Cr}(001)/\mathrm{Al}(001)})/A \quad (1)$$

where $E_{\mathrm{Cr}(001)}$ and $E_{\mathrm{Al}(001)}$ represent the total energies (in units of eV) of the pure Cr and Al plates possessing the (001) surface, respectively. $E_{\mathrm{Cr}(001)/\mathrm{Al}(001)}$ represents the total energy of the Cr(001)/Al(001) interface structure, and A represents the cross-sectional area of the interface. As shown in Figure 2a, the interface structure of bcc (∼0.25 eV/Å^2) was found to be located between the WS values of Cr(001) and Al(001), while

https://doi.org/10.1021/acsomega.3c05827
ACS Omega 2023, 8, 42840−42848

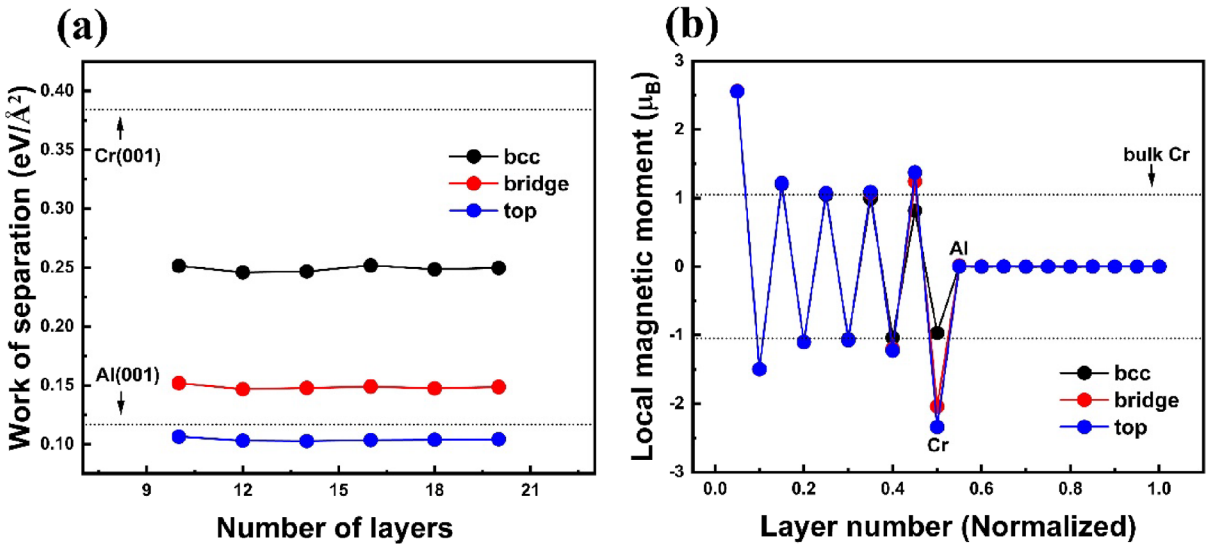

Figure 2. (a) WS value for various Cr(001)/Al(001) interfaces. The interface structures consist of Cr(001) and Al(001) slabs in equal proportions, with different numbers of layers. (b) Local magnetic moment for three distinct types of 20-layer Cr(001)/Al(001) interfaces.

the bridge (~0.15 eV/Å^2) and top (~0.10 eV/Å^2) interface structures were observed to be in close proximity to the WS value of Al(001). This observation suggests that the bcc interface structure may play a distinct role in the interaction between Cr and Al. Furthermore, by subtracting the WS value of the Cr(001)/Al(001) interface from the sum of the surface energies of Cr(001) and Al(001), the interfacial energy can be determined.[22,41−44] This parameter can be used as an indicator of the structural stability of the interface. If the interfacial energy is negative, then it is highly probable that a phase transformation will occur through atomic diffusion between interfaces. The interfacial energy values were calculated for the bcc, bridge, and top interfaces. All the values were found to be positive, with magnitudes of 0.001, 0.203, and 0.293 eV/Å^2, respectively. The low interfacial energy observed at the bcc interface implies the potential for a phase transition to an alternative phase. As shown in Figure 2b, changes were observed in the local magnetic moment of the Cr atom at the interface, occurring in response to the bonding coordination between the Cr and Al atoms. Specifically, in the case of bcc, the local magnetic moment decreased from the surface Cr atoms (~2.56 μ_B) to the bulk level. Despite the Cr−Al bonding at the bridge and top interfaces, the Cr atom at the interface did not exhibit a significant difference from the free surface Cr atom. The findings suggest that the interaction between the Cr and Al atoms can be employed to alter the local magnetic moment of the Cr atom at the interface.

To obtain a comprehensive understanding of the electronic structure with respect to the types of bonds at the interface, the total density of states (DOS) and projected DOS for the Cr(001)/Al(001) structures were examined, as shown in Figure S1. The total DOS exhibited similar trends among all of the considered interfaces. Figure 3a presents the total and projected DOS for the up-spin (top) and down-spin (bottom) of the bcc interface. A comparison of the characteristics of the total and projected DOS revealed that the DOS of the Cr−Al structure is primarily composed of the d orbitals of Cr, with only a minor contribution from the s and p orbitals of Al. This feature is also observed in the local DOS of Cr and Al atoms at the interface (Figure S2). Furthermore, the up- and down-spin DOSs tend to be almost identical. The local DOS was determined by selecting the Cr atom located at the interface, as shown in Figure 3b. The DOS exhibits a distinct pattern in relation to the type of bond between Cr and Al atoms. The DOS below the Fermi level decreases in the following order: bcc, bridge, and top. The order is reversed above an energy of ~1 eV: top, bridge, and bcc. Figure 3c shows the planar-averaged charge density difference $\Delta\rho(z)$ after the formation of the Cr(001)/Al(001) interface relative to that before the formation, which was calculated as follows:

$$\Delta\rho(z) = \Delta\rho(z)_{\mathrm{Cr(001)/Al(001)}} - \Delta\rho(z)_{\mathrm{Cr(001)}} - \Delta\rho(z)_{\mathrm{Al(001)}} \quad (2)$$

Here, $\Delta\rho(z)_{\mathrm{Cr(001)/Al(001)}}$, $\Delta\rho(z)_{\mathrm{Cr(001)}}$, and $\Delta\rho(z)_{\mathrm{Al(001)}}$ present the planar-averaged charge densities of the Cr(001)/Al(001) interface, pure Cr(001) slab, and pure Al(001) slab, respectively. The z axis is perpendicular to the interface. The yellow and cyan regions in the inset of Figure 3c represent the charge accumulation (positive value in $\Delta\rho(z)$) and depletion (negative value), respectively. The significant charge rearrangement occurs primarily between the Cr and Al atoms at the interface. A common characteristic among the interfaces is the occurrence of charge depletion in Cr and Al atoms at the interface, which is accompanied by charge accumulation between the Cr and Al atoms. The configuration of the accumulated charge changes in response to the bonding between Cr and Al atoms at the interface. The charge redistribution at the Cr−Al interface shows a different trend compared to metal−metal interfaces investigated in previous studies.[23,24] This suggests that the charge distribution at the interface can be varied by varying the combination of metals. In Figure 3d, a large amount of charge depletion is noticeable up to the Al−Al interlayer, which is next to the bcc interface. However, for the other interfaces, charge depletion is predominantly observed in the vicinity of the Al atom at the interface. In the case of bcc, the charge distribution exhibits a distinctive three-dimensional morphology resembling that of a mushroom cap. The bridge and top interfaces exhibit cylindrical and spherical shapes, respectively, as illustrated in Figure S3. To conduct a quantitative analysis of the charge transfer, Bader calculations were performed,[45−47] as shown in Figure S4. The Bader charge was determined by subtracting

https://doi.org/10.1021/acsomega.3c05827
ACS Omega 2023, 8, 42840−42848

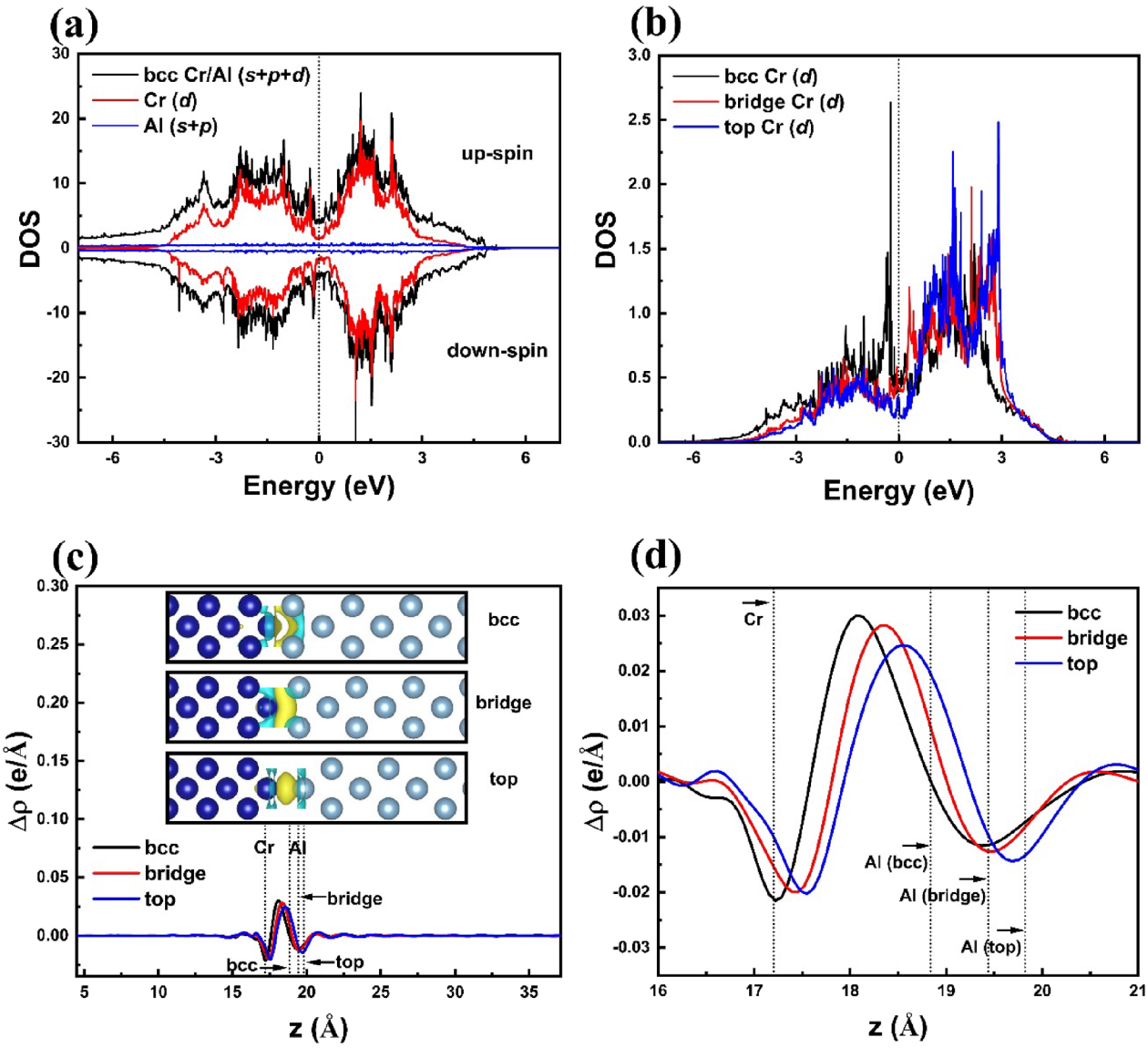

Figure 3. Electronic properties of the bcc, bridge, and top interfaces. (a) Total DOS and the corresponding projected DOS for the bcc Cr(001)/Al(001) interface. (b) Local DOS of the Cr atom adjacent to the Al atom at the bcc interface. The Fermi level was adjusted to 0 eV. (c) Planar-averaged charge density difference along the [001] direction. The isosurfaces are approximately 0.002 e/bohr^3. The yellow and cyan isosurfaces indicate the areas of charge accumulation and depletion, respectively. The visualized charge density difference for the bcc (top), bridge (middle), and top (bottom) interfaces is presented in panel (c). (d) Magnified view of the interface region of panel (c).

the charge of the Cr(001)/Al(001) interface configuration from the charges of the pure Cr(001) and pure Al(001) slabs. Negative and positive Bader charge values signify electron acceptors and donors, respectively. Substantial charge transfer between Cr and Al atoms is solely observed at the bcc interface; the other interfaces hardly exhibit charge transfer.

The mechanical properties of the interface structure were examined through two distinct methodologies. The results of the rigid grain shift (RGS)[48−50] method are shown in Figure 4. This method involves the introduction of vacuum conditions into an arbitrary interlayer followed by self-consistent calculations to obtain the binding energy curve as a function of the displacement. The binding energy was determined by calculating the difference between the total energies before and after the application of vacuum conditions to the interface model. The RGS method is capable of analyzing the mechanical properties of a specific interlayer. In contrast, the homogeneous lattice extension (HLE) method,[51,52] whose results are shown in Figure 5, involves applying mechanical deformation to the entire interface structure and performing relaxation, while fixing the lattice along the in-plane direction, and then determining which interlayer is destroyed. The mechanical properties of the Cr−Al and Al−Al interlayers were analyzed using the RGS method, as shown in the insets of Figure 4a and Figure 4c, respectively. Our DFT results are consistent with the findings of a numerical approach known as the universal binding energy relation.[53−55] The stress−displacement curves for the Cr−Al and Al−Al interlayers were obtained by differentiating the binding energy with respect to the displacement, as shown in Figure 4b and Figure 4d, respectively. The slope, which is also termed the elastic modulus, decreases in the order of bcc, bridge, and top, as illustrated in Figure 4d. Additionally, Figure 4b shows that the bcc interface has the highest theoretical stress, i.e., approximately 23.71 GPa. The bridge and top interfaces exhibit theoretical stresses of approximately 15.63 and 12.03 GPa,

https://doi.org/10.1021/acsomega.3c05827
ACS Omega 2023, 8, 42840−42848

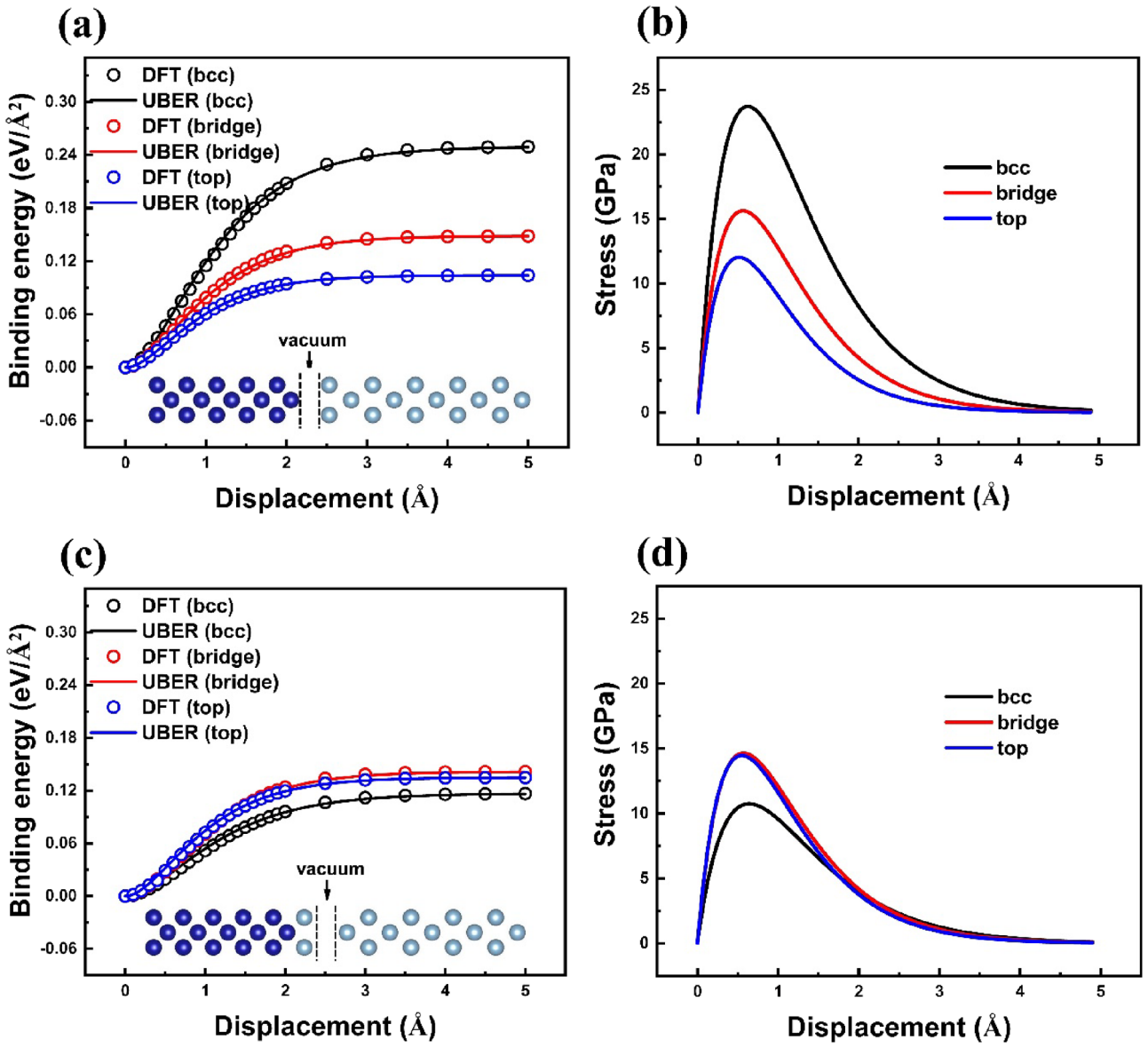

Figure 4. Mechanical responses of interfaces with bcc, bridge, and top configurations. The binding energies of the (a) Cr−Al and (c) Al−Al atoms as a function of the displacement were determined using the RGS method. The insets in parts (a) and (c) indicate the locations where a vacuum condition can be introduced. Stress−displacement relationship at the (b) Cr−Al and (d) Al−Al interlayers.

respectively. The bcc interlayer exhibits a remarkable bond strength, while the Al−Al interlayer in close proximity has a theoretical stress of approximately 10.74 GPa, as shown in Figure 4d. This value is lower than the stress values of the Al−Al interlayer in the bridge and top interfaces, which are approximately 14.64 and 14.45 GPa, respectively. The bcc interface reduces the bond strength of adjacent Al−Al atoms. This finding indicates that the HLE method can predict the destruction at the Al−Al interlayer next to the bcc interface.

For this, the strain−stress curve obtained using the HLE method is shown in Figure 5a. As the magnitude of the applied load increased, the stress gradually increased, ultimately resulting in structural failure. This failure was accompanied by a reduction in stress at homogeneous strains of 0.15 for bcc and 0.16 for bridge and top. In the inset of Figure 5a, under the critical strain (denoted by the arrow), the charge distribution between Al atoms is almost zero for all of the interfaces. The destruction occurs in immediate proximity to the interface in the case of bcc, confirming the previous RGS findings.

Two aspects of the strain−stress curve are worthy of further investigation. First, the three interface structures exhibit comparable curve slopes. Second, although the Cr(001)/Al(001) structure has a WS value lower than that of the pure Al(001) slab, its destruction occurs at the Al−Al interlayer instead of the top interface. Following the application of homogeneous deformation to the structure, the distributions of local strain in each layer of the optimized bcc, bridge, and top structures are shown in Figure 5b−d, respectively. The concept of local strain is defined as the proportion of the difference between the relaxed interlayer distance after homogeneous deformation (d) and the initial interlayer distance (d_0) to the latter (d_0), which is expressed as $(d-d_0)/d_0$. As mentioned previously, the strain−stress curves of the three interface structures appear to be similar even with the application of homogeneous deformation. This is attributed to the fact that

https://doi.org/10.1021/acsomega.3c05827
ACS Omega 2023, 8, 42840−42848

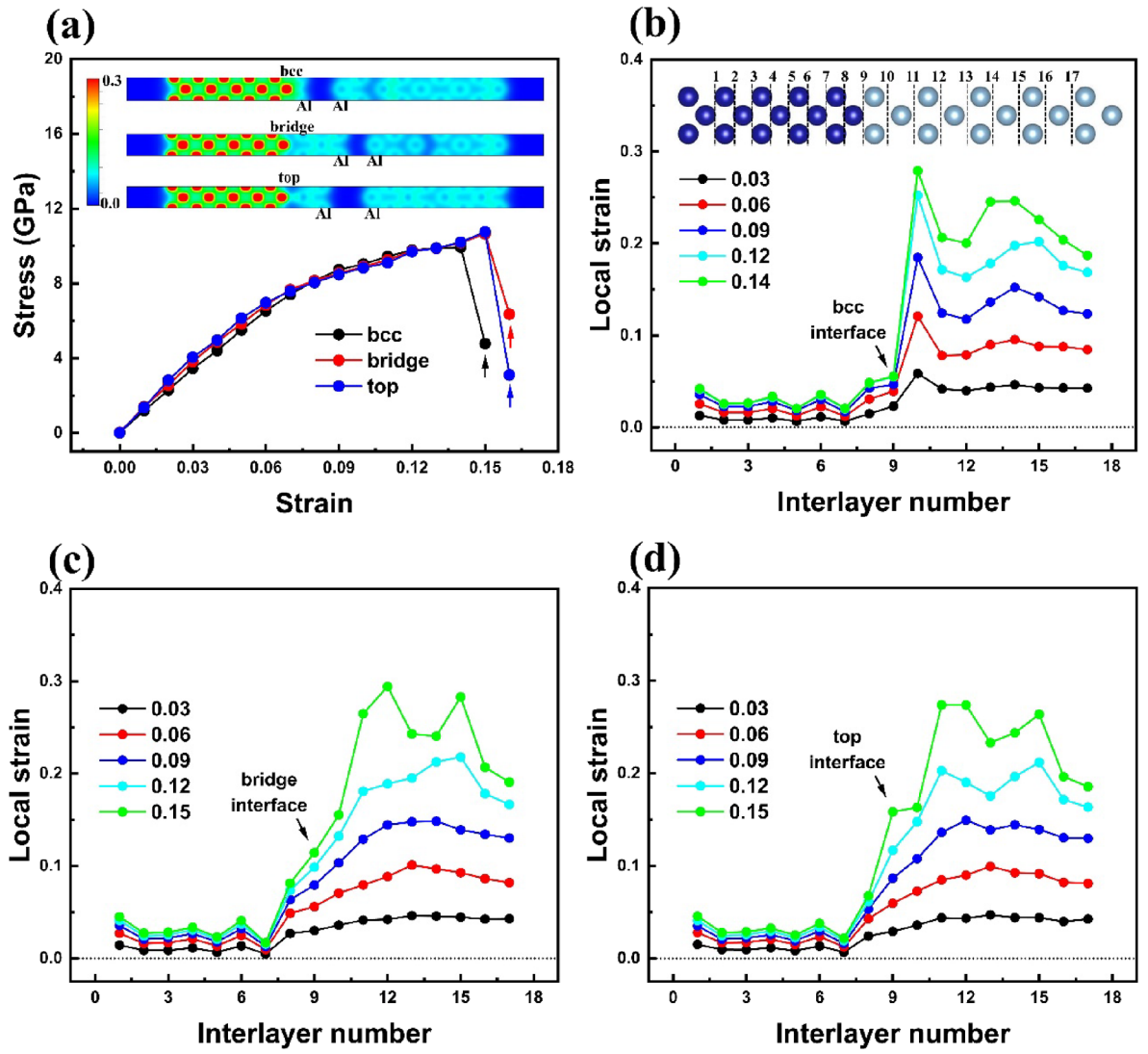

Figure 5. Mechanical properties of interfaces with bcc, bridge, and top configurations. (a) Strain−stress curve obtained by using the HLE method. The charge distribution (in units of e/bohr^3) at failure, which is indicated by an arrow in the mechanical curve, is shown in the inset. The strain distribution for the (b) bcc, (c) bridge, and (d) top interfaces. The inset in panel (b) serves as an indicator of the interlayer number. In this study, the ninth layer was considered as the interface, which is indicated by an arrow in panels (b−d).

the relaxation results in the majority of the deformation being concentrated in the Al matrix. Prior to interlayer separation, a local strain of approximately 30% is observed in the Al region. In particular, it is confirmed that the top interface, which is characterized by the lowest values of WS and stiffness at the interface, experiences a larger strain than the other types of interfaces. In essence, a lower WS and stiffness correspond to a higher probability of deformation. An additional analysis was conducted to determine the energetically favorable interlayer of deformation and to explain why failure occurs at the Al−Al interlayer instead of the top interface with a low WS value. This was done by comparing the total energy differences. Displacement was induced at both the Al−Al and Cr−Al interlayers in the top interface structure using the RGS method, as depicted in the insets of Figure S5a. Figure S5b shows that the maximum stress experienced by the Al−Al interlayer exceeds that of the Cr−Al interlayer. Interestingly, the Al−Al interlayer is more stable than the Cr−Al interlayer at <0.7 Å displacement, as shown in Figure S5c. The displacement of 0.7 Å causes local strains of 0.296 and 0.229 at the Al−Al and Cr−Al interlayers, respectively. Our results imply that uniform deformation is applied to the entire system, but relaxation reduces the local strain at the top interface and increases the deformation at the Al−Al interlayer, causing failure in the Al−Al interlayer of the top interface structure due to the large local strain of approximately 0.3. Thus, the potential for destruction can be evaluated by assessing the concentration of local strain resulting from stiffness rather than relying solely on the WS value.

4. CONCLUSIONS

Spin-polarized DFT calculations were used to analyze the properties of the Cr(001)/Al(001) interface, which has three distinct types: bcc, bridge, and top. It was assumed that Cr has a simple AF arrangement and that using bulk Cr's lattice constant along the in-plane direction would maintain a stable interface structure. The local DOS for the Cr atom at the interface varies slightly near the Fermi level according to its bonding with Al atoms. The Bader charge is exclusively observed at the bcc interface, and it changes the magnetic

https://doi.org/10.1021/acsomega.3c05827
ACS Omega 2023, 8, 42840−42848

configuration of the Cr atom. The bond strength between Cr and Al atoms decreases in the order of the bcc, bridge, and top interfaces according to the WS value and the RGS test. The theoretical stress values for the three structures are 23.71, 15.63, and 10.74 GPa, respectively. The bond strength of the Al−Al interlayer adjacent to the bcc interface decreases significantly, which is attributed to substantial charge transfer from the Al to Cr atom and a wide range of charge depletion. Applying strain through the HLE method results in significant strain concentrated in the Al region following relaxation. Under this condition, the three interface structures have similar mechanical properties, and failure occurs only in the Al−Al interlayer. Moreover, a reduced bond strength in the Al−Al layer near the bcc interface causes destruction with a small strain compared to the other interface structures. The higher stiffness of the Cr−Al interlayer compared to the Al−Al interlayer in the top interface structure prevents destruction despite the lower WS value. The electronic structure of the interface is contingent upon the bonding coordination of Cr and Al atoms, while the mechanical characteristics are predominantly governed by the pliable Al region. These findings can facilitate the design of the Cr−Al structure at the nanoscale. The effect of lattice mismatch and oxidation at the interface will be considered in future work.

■ ASSOCIATED CONTENT

Supporting Information

The Supporting Information is available free of charge at https://pubs.acs.org/doi/10.1021/acsomega.3c05827.

DOS, charge density difference, and Bader charge for different interfaces; comparison of binding energies and strain−stress curves between Cr−Al and Al−Al layers using the RGS method; comparison of total energy for all interface structures using different lattice constants (PDF)

■ AUTHOR INFORMATION

Corresponding Author

Sung Youb Kim − *Graduate School of Carbon Neutrality and Department of Mechanical Engineering, Ulsan National Institute of Science and Technology, Ulsan 44919, Republic of Korea;* orcid.org/0000-0002-9417-4575; Email: sykim@unist.ac.kr

Author

Soon-Dong Park − *Graduate School of Carbon Neutrality, Ulsan National Institute of Science and Technology, Ulsan 44919, Republic of Korea*

Complete contact information is available at: https://pubs.acs.org/10.1021/acsomega.3c05827

Notes

The authors declare no competing financial interest.

■ ACKNOWLEDGMENTS

This work was supported by the Basic Research Laboratory (BRL) program [grant number 2021R1A4A1033224] of the National Research Foundation (NRF) of Korea. We also thank the UNIST Supercomputing Center for providing access to its supercomputing resources.

■ REFERENCES

(1) Altmayer, F. Chromium MACT facts. *Plat. Surf. Finish.* **1995**, *82* (2), 26−27.
(2) Saiddington, J. C.; Hoey, G. R. Crack-free chromium from conventional plating baths. *Plating* **1974**, *61*, 923−930.
(3) Saiddington, J. C. Effect of plating interruptions on the surface appearance of electrodeposited Cr. *Plat. Surf. Finish* **1978**, *65*, 45−49.
(4) Lausmann, G. A. Electrolytically deposited hardchrome. *Surf. Coat. Technol.* **1996**, *86*−*87*, 814−820.
(5) Nriagu, J. O.; Nieboer, E. *Chromium in the natural and human environments*; John Wiley & Sons, 1988.
(6) Warren, D. J.; McMurray, H. N.; de Vooys, A. C. A. Localised SKP studies of cathodic disbondment on chromium/chromium oxide coated steel. *ECS Trans.* **2013**, *50*, 67−78.
(7) Kwon, S. C.; Kim, M.; Park, S. U.; Kim, D. Y.; Kim, D.; Nam, K. S.; Choi, Y. Characterization of intermediate Cr-C layer fabricated by electrodeposition in hexavalent and trivalent chromium baths. *Surf. Coat. Technol.* **2004**, *183*, 151−156.
(8) Wijenberg, J. H. O. J.; Steegh, M.; Aarnts, M. P.; Lammers, K. R.; Mol, J. M. C. Electrodeposition of mixed chromium metal-carbide-oxide coatings from a trivalent chromium-formate electrolyte without a buffering agent. *Electrochim. Acta* **2015**, *173*, 819−826.
(9) Barrera-Díaz, C. E.; Lugo-Lugo, V.; Bilyeu, B. A review of chemical, electrochemical and biological methods for aqueous Cr(VI) reduction. *J. Hazard. Mater.* **2012**, *223*−*224*, 1−12.
(10) Gao, Y.; Chen, Q.; Zhang, S.; Long, H.; Dai, J.; Sun, H.; Chen, C. Enhanced light extraction efficiency of AlGaN-based deep ultraviolet light-emitting diodes by incorporating high-reflective n-type electrode made of Cr/Al. *IEEE Trans. Electron Devices* **2019**, *66*, 2992−2996.
(11) Kaltenbrunner, M.; Adam, G.; Głowacki, E. D.; Drack, M.; Schwödiauer, R.; Leonat, L.; Apaydin, D. H.; Groiss, H.; Scharber, M. C.; White, M. S.; Sariciftci, N. S.; Bauer, S. Flexible high power-per-weight perovskite solar cells with chromium oxide-metal contacts for improved stability in air. *Nat. Mater.* **2015**, *14*, 1032−1039.
(12) Guo, G.; Wang, H. Calculated elastic constants and electronic and magnetic properties of bcc, fcc, and hcp Cr crystals and thin films. *Phys. Rev. B* **2000**, *62*, 5136−5143.
(13) Černý, M. Elastic stability of magnetic crystals under isotropic compression and tension. *Mater. Sci. Eng., A* **2007**, *462*, 432−435.
(14) Ossowski, T.; Kiejna, A. Density functional study of surface properties of chromium. *Surf. Sci.* **2008**, *602*, 517−524.
(15) Habibi, P.; Barreteau, C.; Smogunov, A. Electronic and magnetic structure of the Cr(001) surface. *J. Phys.: Condens. Matter* **2013**, *25*, No. 146002.
(16) Asada, T.; Blügel, S.; Bihlmayer, G. Electronic and magnetic structure of the (001) surfaces of V, Cr, and V/Cr. *Phys. Rev. B* **2000**, *62*, R11937.
(17) Liu, W.; Li, J. C.; Zheng, W. T.; Jiang, Q. NiAl (110) Cr (110) interface: A density functional theory study. *Phys. Rev. B* **2006**, *73*, No. 205421.
(18) Johnson, D. F.; Jiang, D. E.; Carter, E. A. Structure, magnetism, and adhesion at Cr/Fe interfaces from density functional theory. *Surf. Sci.* **2007**, *601*, 699−705.
(19) Fawcett, E. Spin-density-wave antiferromagnetism in chromium. *Rev. Mod. Phys.* **1988**, *60*, 209.
(20) Hafner, R.; Spišák, D.; Lorenz, R.; Hafner, J. Magnetic ground state of Cr in density-functional theory. *Phys. Rev. B* **2002**, *65*, 1844321.
(21) Cottenier, S.; De Vries, B.; Meersschaut, J.; Rots, M. What density-functional theory can tell us about the spin-density wave in Cr. *J. Phys.: Condens. Matter* **2002**, *14*, 3275.
(22) Lu, S.; Hu, Q. M.; Punkkinen, M. P. J.; Johansson, B.; Vitos, L. First-principles study of fcc-Ag/bcc-Fe interfaces. *Phys. Rev. B* **2013**, *87*, No. 224104.
(23) Park, S. D.; Kim, S. Y.; Kim, D. Ab initio investigations of the interfacial bond of Fe(001)/Al(001). *Mater. Today Commun.* **2021**, *26*, No. 102107.

(24) Park, S. D.; Kim, D.; Kim, S. Y. Effect of oxidation on mechanical properties of Ni/Cu interface: A density functional theory study. *Mater. Today Commun.* **2022**, *33*, No. 104307.
(25) Zhang, Y.; Zhang, C.; Zhang, Z.; Dong, N.; Wang, J.; Liu, Y.; Lei, Z.; Han, P. Effects of B on the segregation behavior of Mo at the Fe−Cr(111)/Cr_2O_3(0001) interface: A first-principles study. *Metals* **2020**, *10*, 577.
(26) Yin, X.; Wang, H.; Han, E. H. Cl-induced passivity breakdown in α-Fe_2O_3 (0001), α-Cr_2O_3 (0001), and their interface: A DFT study. *J. Mater. Sci. Technol.* **2022**, *129*, 70−78.
(27) Wang, J.; Zhang, H.; Huang, W.; Lu, Z. Effects of aluminum diffusion on the oxide of the FeCrAl alloys surface: A first−principles study. *Mater. Today Commun.* **2022**, *33*, No. 104594.
(28) Kresse, G.; Furthmüller, J. Efficiency of ab-initio total energy calculations for metals and semiconductors using a plane-wave basis set. *Comput. Mater. Sci.* **1996**, *6*, 15−50.
(29) Kresse, G.; Furthmüller, J. Efficient iterative schemes for ab initio total-energy calculations using a plane-wave basis set. *Phys. Rev. B* **1996**, *54*, 11169.
(30) Kresse, G.; Joubert, D. From ultrasoft pseudopotentials to the projector augmented-wave method. *Phys. Rev. B* **1999**, *59*, 1758.
(31) Perdew, J. P.; Burke, K.; Ernzerhof, M. Generalized gradient approximation made simple. *Phys. Rev. Lett.* **1996**, *77*, 3865.
(32) Monkhorst, H. J.; Pack, J. D. Special points for Brillouin-zone integrations. *Phys. Rev. B* **1976**, *13*, 5188.
(33) Lee, J. Y.; Punkkinen, M. P. J.; Schönecker, S.; Nabi, Z.; Kádas, K.; Zólyomi, V.; Koo, Y. M.; Hu, Q. M.; Ahuja, R.; Johansson, B.; Kollár, J.; Vitos, L.; Kwon, S. K. The surface energy and stress of metals. *Surf. Sci.* **2018**, *674*, 51−68.
(34) Singh-Miller, N. E.; Marzari, N. Surface energies, work functions, and surface relaxations of low-index metallic surfaces from first principles. *Phys. Rev. B* **2009**, *80*, No. 235407.
(35) Clatterbuck, D. M.; Krenn, C. R.; Cohen, M. L.; Morris, J. W. Phonon instabilities and the ideal strength of aluminum. *Phys. Rev. Lett.* **2003**, *91*, No. 135501.
(36) Bolef, D. I.; De Klerk, J. Anomalies in the elastic constants and thermal expansion of chromium single crystals. *Phys. Rev.* **1963**, *129*, 1063.
(37) Kamm, G. N.; Alers, G. A. Low-temperature elastic moduli of aluminum. *J. Appl. Phys.* **1964**, *35*, 327−330.
(38) Griffith, A. A. The phenomena of rupture and flow in solids. *Philos. Trans. R. Soc. London Ser. A* **1921**, *221*, 163−198.
(39) Mills, K. C.; Su, Y. C. Review of surface tension data for metallic elements and alloys: Part 1 - Pure metals. *Int. Mater. Rev.* **2006**, *51*, 329−351.
(40) Tyson, W. R.; Miller, W. R. Surface free energies of solid metals estimation from liquid surface tension measurements. *Surf. Sci.* **1977**, *62*, 267−276.
(41) Li, J.; Yang, Y.; Li, L.; Lou, J.; Luo, X.; Huang, B. Interfacial properties and electronic structure of β-SiC(111)/α-Ti(0001): A first principle study. *J. Appl. Phys.* **2013**, *113*, No. 023516.
(42) Khalid, M. Z.; Friis, J.; Ninive, P. H.; Marthinsen, K.; Strandlie, A. A first-principles study of the Al (001)/Fe(0−11) interface. *Mater. Sci. Forum* **2018**, *941*, 2349−2355.
(43) He, C.; Cheng, M.; Zhang, M.; Zhang, W. X. Interfacial stability and electronic properties of Ag/M (M = Ni, Cu, W, and Pd) and Cu/Cr interfaces. *J. Phys. Chem. C* **2018**, *122*, 17928−17935.
(44) Lee, S. J.; Lee, Y. K.; Soon, A. The austenite/ε martensite interface: A first-principles investigation of the fcc Fe(1 1 1)/hcp Fe(0 0 0 1) system. *Appl. Surf. Sci.* **2012**, *258*, 9977−9981.
(45) Henkelman, G.; Arnaldsson, A.; Jónsson, H. A fast and robust algorithm for Bader decomposition of charge density. *Comput. Mater. Sci.* **2006**, *36*, 354−360.
(46) Sanville, E.; Kenny, S. D.; Smith, R.; Henkelman, G. Improved grid-based algorithm for Bader charge allocation. *J. Comput. Chem.* **2007**, *28*, 899−908.
(47) Tang, W.; Sanville, E.; Henkelman, G. A grid-based bader analysis algorithm without lattice bias. *J. Phys.: Condens. Matter* **2009**, *21*, No. 084204.
(48) Yamaguchi, M. First-principles study on the grain boundary embrittlement of metals by solute segregation: Part I. Iron (Fe)-solute (B, C, P, and S) systems. *Metall. Mater. Trans. A* **2011**, *42*, 319−329.
(49) Khalid, M. Z.; Friis, J.; Ninive, P. H.; Marthinsen, K.; Strandlie, A. Ab-initio study of atomic structure and mechanical behaviour of Al/Fe intermetallic interfaces. *Comput. Mater. Sci.* **2020**, *174*, No. 109481.
(50) Khalid, M. Z.; Friis, J.; Ninive, P. H.; Marthinsen, K.; Strandlie, A. First-principles study of tensile and shear strength of Fe-Al and α-AlFeSi intermetallic compound interfaces. *Comput. Mater. Sci.* **2021**, *187*, No. 110058.
(51) Černý, M.; Šesták, P.; Rehák, P.; Všianská, M.; Šob, M. Atomistic approaches to cleavage of interfaces. *Model. Simul. Mater. Sci. Eng.* **2019**, *27*, No. 035007.
(52) Qiu, C.; Su, Y.; Chen, B.; Yang, J.; Li, Z.; Ouyang, Q.; Guo, Q.; Xiong, D.; Zhang, D. First-principles investigation of interfacial stability, mechanical behavior and failure mechanism of β-SiC(111)/Al(111) interfaces. *Comput. Mater. Sci.* **2020**, *175*, No. 109608.
(53) Rose, J. H.; Ferrante, J.; Smith, J. R. Universal binding energy curves for metals and bimetallic interfaces. *Phys. Rev. Lett.* **1981**, *47*, 675.
(54) Janisch, R.; Ahmed, N.; Hartmaier, A. Ab initio tensile tests of Al bulk crystals and grain boundaries: Universality of mechanical behavior. *Phys. Rev. B* **2010**, *81*, No. 184108.
(55) Lazar, P.; Podloucky, R. Cleavage fracture of a crystal: Density functional theory calculations based on a model which includes structural relaxations. *Phys. Rev. B* **2008**, *78*, No. 104114.

https://doi.org/10.1021/acsomega.3c05827
ACS Omega 2023, 8, 42840−42848